Cell Calcium 77 (2019) 49–57

Contents lists available at ScienceDirect

Cell Calcium

journal homepage: www.elsevier.com/locate/ceca

Calcium extrusion mechanisms in dendrites of mouse hippocampal CA1 inhibitory interneurons

Simon Chamberland[a], Alfonsa Zamora Moratalla[a,b], Lisa Topolnik[a,b,*]

[a] Department of Biochemistry, Microbiology and Bio-Informatics, Faculty of Science and Engineering, Laval University, Québec, PQ, Canada
[b] Neuroscience Axis, CHU de Québec Research Center, Laval University, Québec, PQ, Canada

ARTICLE INFO

Keywords:
Inhibition
GABAergic interneuron
Plasma membrane calcium ATPase
Sodium-calcium exchanger
SERCA
Mitochondria calcium uniporter

ABSTRACT

Local circuit GABAergic inhibitory interneurons control the integration and transfer of information in many brain regions. Several different forms of plasticity reported at interneuron excitatory synapses are triggered by cell- and synapse-specific postsynaptic calcium (Ca^{2+}) mechanisms. To support this function, the spatiotemporal dynamics of dendritic Ca^{2+} elevations must be tightly regulated. While the dynamics of postsynaptic Ca^{2+} signaling through activation of different Ca^{2+} sources has been explored, the Ca^{2+} extrusion mechanisms that operate in interneuron dendrites during different patterns of activity remain largely unknown. Using a combination of whole-cell patch-clamp recordings and two-photon Ca^{2+} imaging in acute mouse hippocampal slices, we characterized the Ca^{2+} extrusion mechanisms activated by Ca^{2+} transients (CaTs) associated with back-propagating action potentials (bAPs) in dendrites of hippocampal CA1 stratum radiatum interneurons. Our data showed that Ca^{2+} clearance increased as a function of activity, pointing to an activity-dependent recruitment of specific Ca^{2+} extrusion mechanisms. bAP-CaTs were significantly prolonged in the presence of the plasma membrane Ca^{2+} ATPase (PMCA) and Na^{+}/Ca^{2+} exchanger (NCX) inhibitors as well as the sarco/endoplasmic reticulum Ca^{2+} ATPase (SERCA) and the mitochondria Ca^{2+} uniporter (MCU) blockers. While PMCA, NCX and SERCA pumps cooperated in the cytosolic Ca^{2+} removal at a wide range of concentrations, the MCU was only activated at higher Ca^{2+} loads produced by repetitive interneuron firing. These results identify a division of labor between distinct Ca^{2+} extrusion mechanisms shaping dendritic Ca^{2+} dynamics and possibly contributing to activity-dependent regulation of synaptic inputs in interneurons. In addition, the MCU activated by larger Ca^{2+} levels may be involved in the activity-dependent ATP production or interneuron-selective vulnerability associated with cytosolic Ca^{2+} overloads under pathological conditions.

1. Introduction

In neuronal dendrites, the magnitude and spatiotemporal properties of intracellular calcium (Ca^{2+}) elevations control integration of afferent inputs, induction and maintenance of synaptic plasticity, local release of signaling molecules and neuronal excitability. The intracellular Ca^{2+} signals are shaped by dynamic interactions between the sources of Ca^{2+} ion influx, endogenous Ca^{2+} buffers and Ca^{2+} extrusion mechanisms [1–3]. While dendritic Ca^{2+} sources and buffering mechanisms have been well characterized in different cell types, relatively little is known about the distribution and activation of different Ca^{2+} extrusion mechanisms. In fact, much of our knowledge regarding the intracellular Ca^{2+} clearance comes from studies on skeletal and cardiac muscles and peripheral tissues, which show that Ca^{2+} homeostasis is maintained through operation of several mechanisms, including the plasma membrane Ca^{2+} ATPase (PMCA), the plasma membrane Na^{+}/Ca^{2+} exchanger (NCX), the sarco/endoplasmic reticulum Ca^{2+} ATPase (SERCA) and the mitochondria Ca^{2+} uniporter (MCU) [4–8]. These mechanisms exhibit the tissue- and cell type-specific distribution and different affinities for Ca^{2+} ions [9,10], which can be well suited to balance different Ca^{2+} loads during specific patterns of cellular activity.

In particular, the PMCA, SERCA and NCX are considered as the main regulators of the intracellular Ca^{2+} homeostasis that complement each other in terms of Ca^{2+} affinities and transport capacity [11,12]. Similar to the SERCA pump, a high-affinity transporter loading Ca^{2+} to the internal stores and maintaining the low basal cytosolic Ca^{2+} concentration [13], the low-capacity PMCA, which is regulated by

* Corresponding author at: Department of Biochemistry, Microbiology and Bio-Informatics, Faculty of Science and Engineering, Laval University, Québec, PQ, Canada.
E-mail address: lisa.topolnik@bcm.ulaval.ca (L. Topolnik).

https://doi.org/10.1016/j.ceca.2018.12.002
Received 6 September 2018; Received in revised form 25 November 2018; Accepted 3 December 2018
Available online 04 December 2018

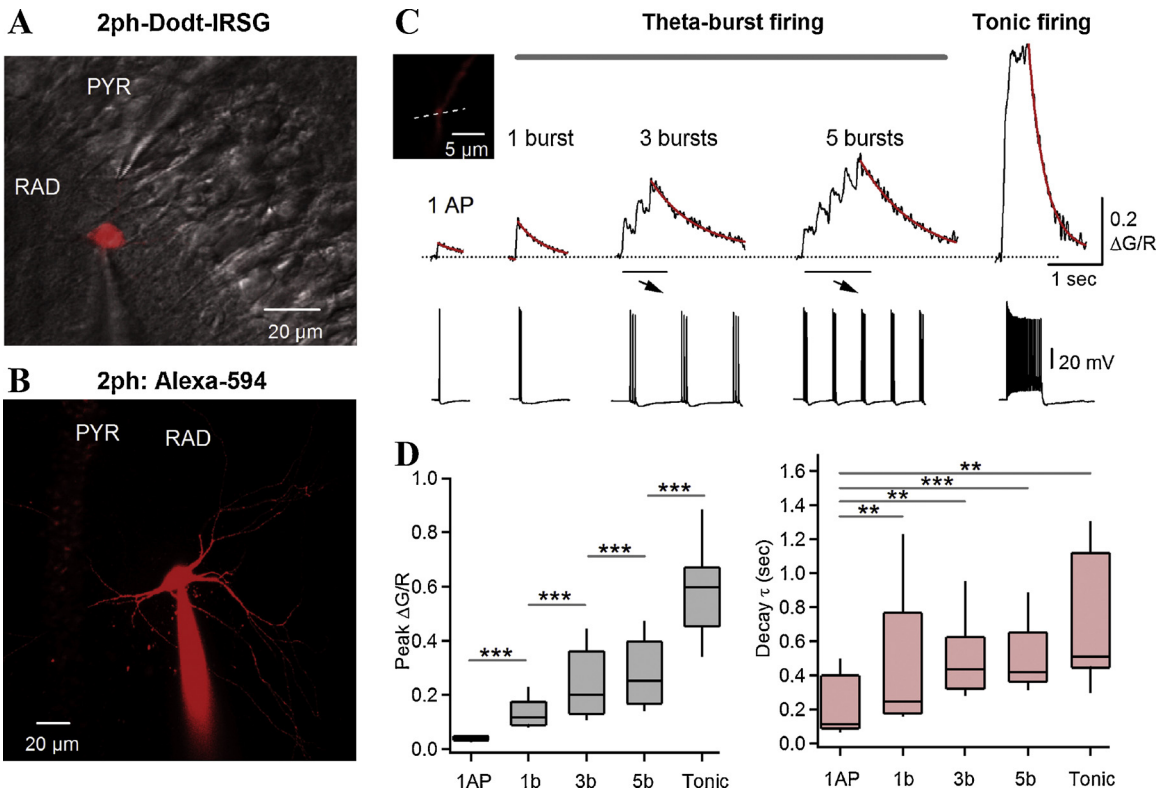

Fig. 1. Two-photon imaging of the backpropagating action potential-evoked Ca^{2+} transients (bAP-CaTs) in dendrites of hippocampal CA1 interneurons. (A) Two-photon Dodt-IRSG image of the CA1 RAD/PYR border illustrating the cell of interest filled with Alexa-594 and Fluo-5 F during whole-cell patch-clamp recording. (B) Two-photon maximal projection image of the CA1 RAD interneuron filled with Alexa-594. (C) Representative examples of bAP-CaTs (top) evoked by different patterns of activity (bottom): a single AP (1 A P), a burst of 3 APs (1 burst), 3 bursts of 3 APs (3 bursts), 5 bursts of 3 APs (5 bursts) and tonic firing (80–100 Hz, 1 s). Red lines on CaT traces correspond to single exponential fits. An inset on top left illustrates a proximal dendritic branch with a linescan location indicated with dotted white line. (D) Box plots of the bAP-CaT peak amplitude (left) and decay time constant (right) recorded during different activity patterns. $^{**}P < 0.01$, $^{***}P < 0.001$, ANOVA.

calmodulin [14,15], has been traditionally seen as a high affinity Ca^{2+} transporter activated mostly at rest by low cytosolic Ca^{2+} fluctuations (100–200 nM). However, numerous PMCA isoforms and splicing variants are also able to extrude Ca^{2+} in the µM range [16]. In contrast, the high-capacity NCX shows a lower Ca^{2+} affinity [17] and is typically activated when Ca^{2+} elevations exceed 200 nM during higher patterns of cellular activity. In addition, the MCU, a calcium-selective channel of the inner mitochondria membrane, which is able to accumulate large amounts of Ca^{2+} within mitochondria matrix during global Ca^{2+} signals, provides for activity-dependent regulation of intracellular Ca^{2+} level [18,19]. Specifically, the sigmoidal response of the MCU to cytosolic Ca^{2+} loads, with a very low activation rate at rest and a large carrying capacity at higher Ca^{2+} concentration [20], represents a supplementary mechanism for Ca^{2+} homeostasis in response to high-activity cellular demands.

In central neurons, the PMCA, SERCA and NCX have been involved in control of pre- and postsynaptic Ca^{2+} dynamics, with direct impact on Ca^{2+}-dependent signaling and synaptic plasticity [12,21,22]. The MCU-mediated Ca^{2+} uptake could modulate synaptic vesicle recycling and ATP production or mediate excitotoxicity through activation of the apoptotic cascade [23–26]. The potential role of these mechanisms in shaping dendritic Ca^{2+} gradients and synaptic plasticity has been investigated in details in cerebellar Purkinje cells and hippocampal CA1 pyramidal neurons [12,27]. Yet, very little is known regarding the Ca^{2+} extrusion mechanisms in GABAergic inhibitory interneurons. As dendrites of these cells exhibit specific structural (e.g., absence of spines, large content of mitochondria; [28]) and functional (e.g., high endogenous Ca^{2+} binding capacity, [29]; high Ca^{2+} compartmentalization, [30]) organization, detailed analysis of dendritic Ca^{2+} signaling, including Ca^{2+} clearance, is required for understanding the interneuron-specific forms of Ca^{2+}-dependent synaptic plasticity [31]. Here, we analyzed the Ca^{2+} extrusion mechanisms that operate in dendrites of hippocampal CA1 inhibitory interneurons. Our data indicate that the PMCA, SERCA, NCX and MCU all play a role in regulation of dendritic Ca^{2+} homeostasis, with contribution of each mechanism determined by the interneuron activity pattern.

2. Materials and methods

2.1. Ethics statement

All experiments were carried out in accordance with the animal welfare guidelines of the Animal Protection Committee of the Université Laval (CPAUL) and the Canadian Council on Animal Care. The protocol was approved by the CPAUL.

2.2. Slice preparation

Transverse hippocampal slices were obtained from P15–23 C57B1/J6 mice (Charles River, St. Laurent, Quebec, Canada). Animals were deeply anesthetized with isoflurane (open-drop exposure within a tightly-closed glass bell jar; 1cc/500 cc jar volume) and decapitated. The brain was rapidly removed into ice-cold, oxygenated "cutting" solution containing (in mM): 250 sucrose, 2 KCl, 1.25 NaH_2PO_4, 26 $NaHCO_3$, 7 $MgSO_4$, 0.5 $CaCl_2$, and 10 glucose, pH 7.4, 320–340 mOsm. Slices (300 µm thick) were cut using a VT1000S Vibratome (Leica Microsystems Inc., Germany), and then transferred to a heated (35 °C) oxygenated solution containing (in mM): 124 NaCl, 2.5 KCl, 1.25

NaH_2PO_4, 26 $NaHCO_3$, 3 $MgSO_4$, 1 $CaCl_2$, and 10 glucose for recovery (30 min), following which they were kept at room temperature until use.

2.3. Electrophysiological recordings, two-photon Ca^{2+} imaging and pharmacology

During experiments, individual slices were transferred to a recording chamber and perfused continuously (2.5 ml/min) with artificial cerebrospinal fluid (ACSF) containing (in mM): 124 NaCl, 2.5 KCl, 1.25 NaH_2PO_4, 26 $NaHCO_3$, 2 $MgSO_4$, 2 $CaCl_2$, and 10 glucose, saturated with 95% O_2 and 5% CO_2 (295–305 mOsm) at 31 ± 2.0 °C. In some experiments, ACSF containing 100 mM LiCl and 24 mM NaCl instead of 124 mM NaCl or ACSF containing cyclopiazonic acid (CPA, 30 μM) was used. Identification of hippocampal CA1 stratum radiatum (RAD) interneurons was performed using a 40x objective and infrared video microscopy with the aid of the CCD camera (70 Series; Dage-MTI, Michigan City, IN) mounted on an upright multiphoton confocal laser-scanning microscope Leica TCS SP5 (Leica Microsystems, Germany) or using two-photon Dodt infrared scanning gradient microscopy (Fig. 1A; Leica Microsystems Inc., Germany).

Whole-cell patch-clamp recordings were performed in current-clamp mode at a holding potential of −60 mV. Recording electrodes (3–5 MΩ) pulled from borosilicate glass (World Precision Instruments, Sarasota, FL, USA) were filled with a solution containing (in mM): 130 $KMeSO_3$, 2 $MgCl_2$, 10 diNa-phosphocreatine, 10 HEPES, 2 ATPtris (or 4 ATP-Mg), 0.4 GTPTris, 0.01 Alexa-594 and Ca^{2+}-sensitive indicator (0.3 mM, Fluo-5 F, K_D = 1.3 μM, κ_{Dye} = 230.8; or 0.2 mM Oregon Green 488 BAPTA-1, K_D = 170 nM, κ_{Dye} = 1 176.5; or 0.5 mM Oregon Green 488 BAPTA-5 N, K_D = 20 μM, κ_{Dye} = 25; ThermoFisher), pH 7.25–7.35, 275–285 mOsm. The added buffer capacity (κ_{Dye}) of calcium indicators were approximated as:

$$\kappa_{Dye} = [Dye]/ K_D;$$

where [Dye] is the dye concentration, and K_D is the corresponding dissociation constant.

In some experiments, calmidazolium (20 μM) or Ru360 (1 μM) were included in the intracellular recording solution. Data acquisition (filtered at 2 kHz, digitized at 10 kHz) were performed using a MultiClamp 700B amplifier, a Digidata1440 digitizer and pClamp10.2 software (Molecular Devices, Sunnyvale, CA). Cells with unstable bridge balance (changes > 10%) or holding current exceeding 100 pA were rejected.

Dendritic Ca^{2+} imaging was performed as described previously [32,33] using two-photon excitation laser scanning microscope Leica TCS SP5 (Leica Microsystems Inc., Germany) based on a mode-locked Ti:Sapphire laser (Chameleon Ultra-II) operating at 800 nm wavelength, 80 MHz pulse repeat, < 200 fs pulse width (Coherent, Santa Clara, CA, USA). A long-range water-immersion objective (40x; numerical aperture, 0.8) was used. Fluorescence was detected through a short-pass filter (cut-off = 680 nm) using external non-descanned detectors, and images were acquired using LAS SP5 software (Leica Microsystems Inc., Germany). Red fluorescence of Alexa-594 was used to locate primary or secondary dendrites at 10–120 μm from the soma (Figs. 1,2). To monitor changes in intracellular Ca^{2+} concentration associated with action potentials, green and red fluorescence was collected at 1 min intervals by scanning a line (500 Hz) across the dendrite of interest (total length, ~2–3 μm). The line position was checked regularly and adjusted for possible drift. The current study was done under different dye loading conditions (45–60 min *vs* 20–30 min in [34]) to assure the appropriate drug concentration (calmidazolium and Ru360) in dendrites at 20–50 μm from soma.

To test for the activity-dependent regulation of Ca^{2+} extrusion mechanisms, we examined the amplitude and decay time constant of Ca^{2+} transients evoked by backpropagating action potentials (bAP-CaTs) under different stimulation protocols, mimicking in vivo network activity in the hippocampus: single APs, theta-burst stimulation [1, 3 or 5 bursts of APs at 200 ms intervals (5 Hz), each burst consisting of 3 APs at 100 Hz] and tonic firing (100–120 Hz, 1 s) evoked by somatic current injection (800 pA, 3–5 ms for single APs; 300–500 pA, 1 s for tonic firing).

2.4. Data analysis

Ca^{2+} imaging and electrophysiological recordings were analyzed using the TCS SP5 software, Clampfit 10.2 (Molecular Devices, Sunnyvale, CA) and IgorPro 4.2 (Wavemetrics, Lake Oswego, OR, USA). For analysis of Ca^{2+} transients, changes in fluorescence were calculated relative to the fluorescence intensity of Ca^{2+} insensitive dye and expressed as $\Delta G/R = (G - G_{rest})/R$, where R –average red fluorescence reported by Alexa-594, G_{rest} and G – green fluorescence reported by Ca^{2+} indicator prior and after (peak value) stimulation, respectively. The peak amplitude and decay kinetics (single exponential fit) of Ca^{2+} transients were measured to assess the kinetic properties of Ca^{2+} extrusion in different conditions. Statistical analysis was performed using Kolmogorov-Smirnov test (for data distribution), *t*-test (paired or unpaired), Mann-Whitney and ANOVA test. The data is presented as mean ± SE or as median with interquartile intervals (Fig. 1D).

2.5. Immunohistochemistry

Biocytin (0.15-0.2%) (Sigma) was routinely added to the internal patch solution to allow cell labeling and reconstruction. Slices containing biocytin-filled cells were fixed (4% paraformaldehyde in 0.1 M phosphate buffer) overnight at 4 °C, and rinsed in TBS. The slices then were permeabilized (0.25% Triton) and incubated with Alexa-546-conjugated streptavidin (1:200, Molecular Probes, Eugene, OR, USA). After multiple washes, slices were mounted using fluorescence mounting medium (DAKO). Three-dimensional anatomical reconstructions of recorded neurons were performed using confocal laser scanning microscope Leica TCS SP5 (Leica Microsystems, Germany). Final maximal projections of the Z-stacks (acquired with a 1-μm step) containing different parts of neuronal processes were merged using Adobe Photoshop CS3 (Adobe Systems, San Jose, CA).

3. Results

To examine the kinetics of Ca^{2+} extrusion in dendrites of hippocampal CA1 RAD interneurons, we studied Ca^{2+} transients evoked by backpropagating action potentials (bAP-CaTs) using two-photon Ca^{2+} imaging in combination with patch-clamp whole-cell recordings (Fig. 1A, B). The data was obtained from 112 RAD interneurons, which were identified *post hoc* as either basket cells (BCs; n = 49) or the Schaffer-collateral-associated cells (SC-ACs; n = 45) (Fig. 2A), with the rest (n = 18 cells) being unidentified due to the cut axon. For Ca^{2+} imaging, cells were loaded with a morphological dye Alexa-594 (10 μM) and a Ca^{2+} -sensitive medium-affinity indicator Fluo-5 F (300 μM) for 45–60 min before imaging. Such loading duration was necessary to achieve the appropriate concentration of pharmacological compounds, which were included in the intracellular solution in some experiments (Calmidazolium, Ru360; Fig. 5). Ca^{2+} imaging was performed in proximal dendrites (20–50 μm from soma), except for propagation experiments where bAP-CaTs were examined along the entire dendritic tree at 10 to 160 μm from soma (Fig. 2C–E). Somatic current injections were used to evoke single APs (0.8–1 nA, 3–5 ms), bursts of APs (1, 3 or 5 bursts of 3 APs at 5 Hz with 10-ms inter-spike interval within the burst) or tonic firing (80–100 Hz, 1 s), and associated bAP-CaTs were examined (Fig. 1C). As the decay of bAP-CaTs reflects the rate of Ca^{2+} ion extrusion from the cytoplasm and may affect the magnitude of local Ca^{2+} elevations [12], we analyzed the decay time constant of bAP-CaTs as well as their peak amplitude.

Consistent with high intracellular Ca^{2+} binding capacity due to

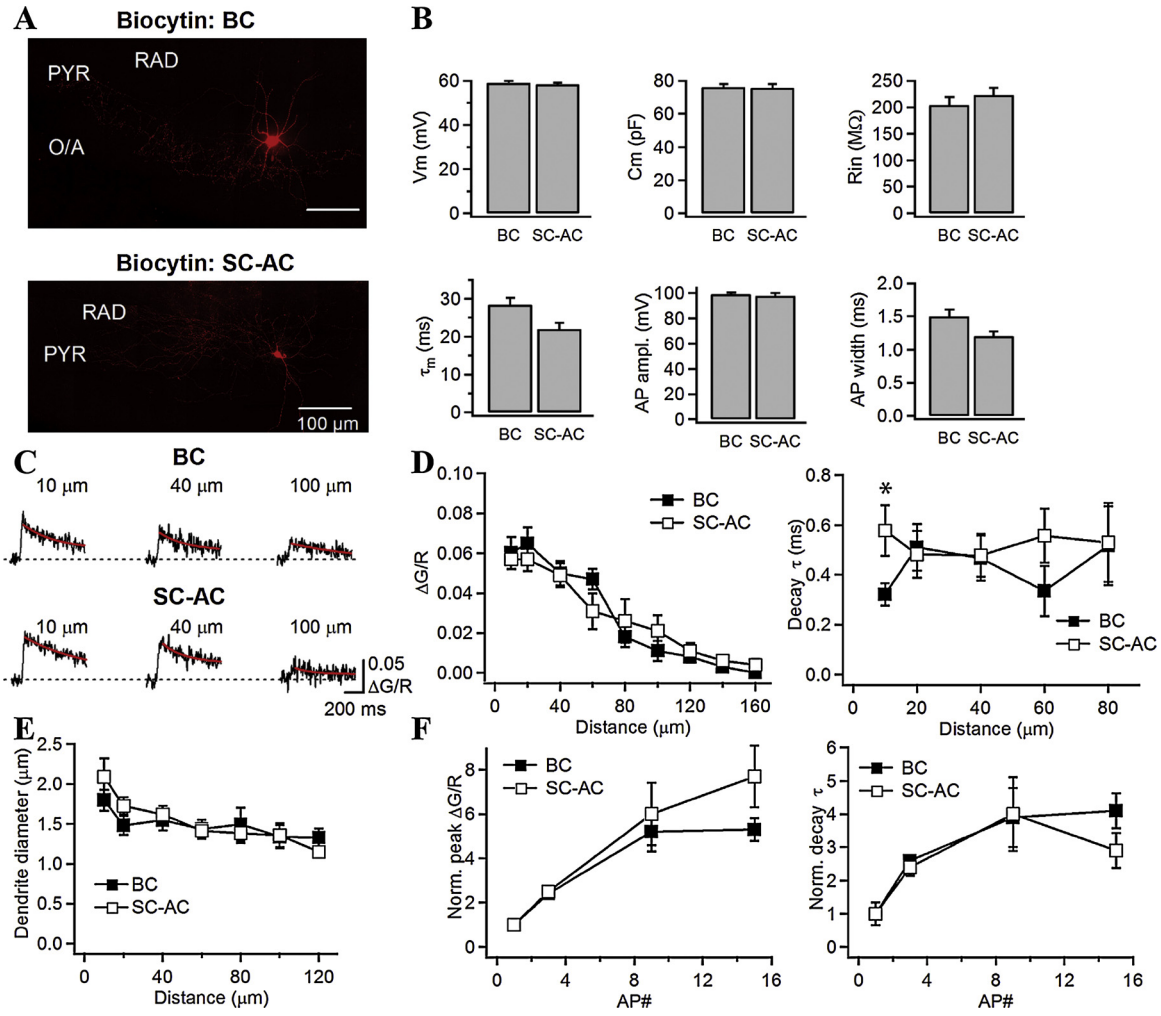

Fig. 2. Cell-specific properties of membrane parameters and dendritic bAP-CaTs.
(A) Confocal images of recorded interneurons filled with biocytin: top, basket cell (BC); bottom, Schaffer-collateral-associated cell (SC-AC). (B) Summary bar graphs for passive and active membrane properties of BCs (n = 49) and SC-ACs (n = 45). (C) Sample traces of dendritic bAP-CaTs evoked by a burst of 3 APs at different distance from soma in BCs (top) and SC-ACs (bottom). Red lines on CaT traces correspond to single exponential fits. (D) Summary graphs illustrating changes in the bAP-CaT peak amplitude (ΔG/R, left) and decay time constant (right) as a function of distance from soma in BCs (n = 8) and SC-ACs (n = 7). Note a slower decay τ in SC-ACs at 10 µm from soma. *$P < 0.05$, Mann-Whitney test. (E) Summary plot showing the BC (n = 8) *vs* SC-AC (n = 7) dendrite diameter at different distances from the soma. (F) Summary graphs illustrating changes in the bAP-CaT peak amplitude (ΔG/R, left) and decay time constant (right) as a function of the AP number: 1bAP (BC, n = 10; SC-AC, n = 7), 3 bAPs (BC, n = 10; SC-AC, n = 7), 9 bAPs (BC, n = 7; SC-AC, n = 7), 15 bAPs (BC, n = 7; SC-AC, n = 7). No significant difference was observed between the BCs and SC-ACs at any number of bAPs ($P > 0.05$, ANOVA).

prolonged loading with exogenous Ca^{2+} buffer and a relatively high endogenous Ca^{2+} buffer capacity in interneurons [2,12,29,34,35], bAP-CaTs evoked by a single AP under our experimental conditions had a small amplitude and a relatively slow decay time constant (ΔG/R peak amplitude: 0.04 ± 0.001, decay τ: 233.5 ± 61 ms, n = 22; Fig. 1D). Increasing the number of APs to 3 resulted in a significant increase of both the bAP-CaT peak amplitude and decay τ (ΔG/R peak amplitude: 0.14 ± 0.02, n = 13, $P < 0.001$; decay τ: 588 ± 65 ms, n = 13, $P < 0.01$, ANOVA; Fig. 1D). To further explore the rates of Ca^{2+} clearance and, as a consequence, the magnitude of Ca^{2+} elevations during theta-like interneuron firing that is observed in vivo [36], we next evoked 3 APs in bursts (3 and 5 bursts; Fig. 1C, center). While the peak amplitude of bAP-CaTs continued to increase in this case (3burst-ΔG/R: 0.24 ± 0.04, 5burst-ΔG/R: 0.28 ± 0.04, n = 13, $P < 0.001$, ANOVA), the decay time constant was similar to that evoked by a single burst of 3 APs (1burst-decay τ: 509 ± 125 ms, 3burst-decay τ: 527 ± 80 ms, 5burst-decay τ: 514 ± 58, n = 13, $P > 0.05$, ANOVA; Fig. 1D, right), indicating that additional Ca^{2+} extrusion mechanisms were likely activated during repetitive bursting activity to confine dendritic Ca^{2+} elevations. To verify this assumption, we further increased the activity level by inducing a tonic firing (80–100 Hz) in interneurons for 1 s (Fig. 1C, right). Surprisingly, bAP-CaTs increased significantly in their peak amplitude (ΔG/R peak amplitude: 0.61 ± 0.05, n = 20, $P < 0.001$, ANOVA; Fig. 1D, left) but not in their decay (decay τ: 614 ± 76 ms, n = 20, $P > 0.05$, ANOVA; Fig. 1D, right). In summary, the kinetics of Ca^{2+} extrusion increased significantly with changes in firing from 1 AP to 1 burst of 3 APs, but then remained unchanged at all patterns of activity tested. It is to be noted that a medium-affinity dye Fluo-5 F can saturate under high levels of activity. However, in our experiments, the peak amplitude of the CaTs evoked by 1 AP, 3 APs, 3 bursts, 5 bursts and tonic stimulation reported in Fig.1C were all significantly different from each other. Therefore, the decay time constant of the CaTs could be measured and compared across the stimulation protocols to reach conclusions about the Ca^{2+} decay kinetics and extrusion in interneurons.

As dendritic bAP-CaTs may exhibit the cell type-specific properties depending on the cell membrane parameters and dendritic Ca^{2+} mechanisms, we next examined the membrane and the bAP-CaT properties

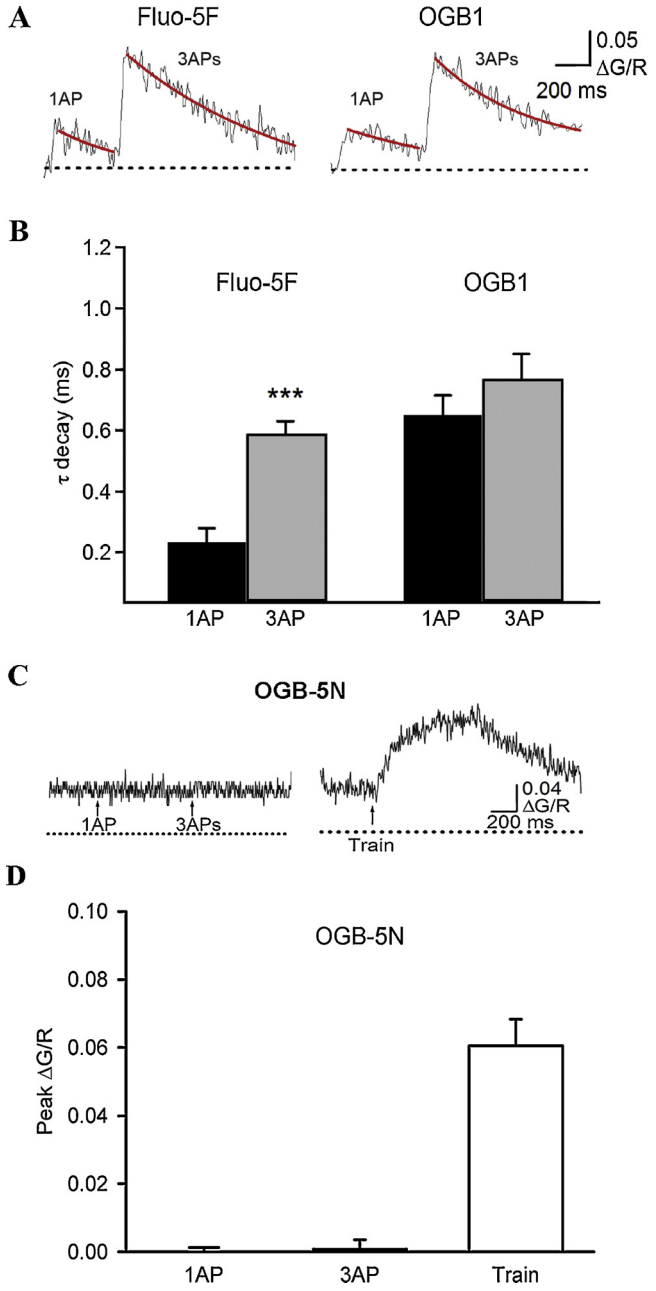

Fig. 3. Calcium-dependent slowing of bAP-CaTs in dendrites of hippocampal CA1 interneurons.

(A) Representative traces of bAP-CaTs evoked by single and three APs when using a medium affinity Fluo-5 F (left) or a high affinity Oregon Green BAPTA-1 (OGB1, right) Ca^{2+} indicators. Red lines on CaT traces correspond to single exponential fits. (B) Summary bar graphs showing changes in decay time constant of bAP-CaTs under two imaging conditions. Note a significant slowing down of the bAP-CaT decay with increase in the AP number when a lower affinity Ca^{2+} indicator was used, and the absence of this phenomenon in the presence of a high affinity OGB1. (C) Representative traces of bAP-CaTs evoked by single and three APs or AP train when using a low affinity OGB-5 N. (D) summary bar graphs showing no detectable CaT for 1 AP and 3 APs and small amplitude CaTs in response to trains of APs.

in BC *vs* SC-ACs (Fig. 2). Consistent with previous report [34], except the difference in the I_h current, BCs and SC-ACs had similar passive and active membrane properties (Fig. 2A, B). The diameter of dendrites was also similar between the two cell types (Fig. 2E). Furthermore, in both cell types the bAP-CaTs' amplitude declined with distance from soma (Fig. 2C; D, left) but their decay remained relatively constant (except at distances ≤10 µm from soma, where it was slower in the SC-ACs than in BCs, $^*P < 0.05$, Mann-Whitney test; Fig. 2D, right; [34]). In addition, both cell types demonstrated a similar activity-dependent increase in the bAP-CaTs' amplitude and decay (Fig. 2F). Accordingly, for the rest of this study, the data from all cells were pooled together to identify the common mechanisms responsible for the activity-dependent dendritic Ca^{2+} removal in these cells.

To examine whether the activity-dependent slow-down of bAP-CaTs in response to the increased number of bAPs (Fig. 1D, right) was dependent on the intracellular Ca^{2+} level [12], we performed Ca^{2+} imaging experiments using a high-affinity Ca^{2+} indicator Oregon Green 488 BAPTA 1 (OGB1, 200 µM; K_D = 170 nM; Fig. 3A). This experimental condition increased the Ca^{2+} buffering capacity imposed by the dye by a factor of ~5 (see Material and Methods), further constraining the increase in intracellular Ca^{2+}. Under these conditions, single bAP-evoked CaTs had a significantly slower decay (OGB1 1bAP-CaT decay τ: 648.5 ± 106 ms, n = 6 *vs* Fluo-5 F 1bAP-CaT decay τ: 233 ± 61 ms, n = 22; Fig. 3B; $P < 0.05$, ANOVA), which remained unchanged with a larger number of APs (Fig. 3B). Here, we note that the decay kinetics of the CaTs recorded with OGB-1 are slower than those recorded with Fluo-5 F. This is expected given the different Koff of Fluo-5 F vs. OGB-1 and the ~5 fold larger exogenous buffering capacity imposed by the OGB-1 concentration, which is an important validation of our experimental conditions. Given that the 1 AP CaT decay time constant was not different from the 3 APs decay time constant when recordings were performed with OGB-1, but the CaTs decay time constant was significantly different between 1 AP and 3 APs when experiments were performed with Fluo-5 F, we conclude that the bAP-CaT decay prolongation requires increase in the intracellular Ca^{2+}. It is to be noted that using a low affinity Ca^{2+} indicator Oregon Green 488 BAPTA 5 N (OGB-5 N, 500 µM; K_D = 20 µM; Fig. 3C, D), to rule out any potential effect of dye saturation in these protocols, was not successful in detecting small CaTs evoked by 1 AP (ΔG/R peak amplitude: -0.001 ± 0.002, n = 13) and 3 APs (ΔG/R peak amplitude: 0.0008 ± 0.0003, n = 13; Fig. 3C, D) and could only detect bAP-CaTs associated with a train of APs (ΔG/R peak amplitude: 0.06 ± 0.007, n = 8 cells; Fig. 3C, D), indicating that it could not be used for comparison of Ca^{2+} extrusion between different patterns of AP firing in interneurons.

To determine the mechanisms responsible for Ca^{2+} extrusion in dendrites of interneurons, we examined the roles of the PMCA, the NCX, the SERCA pump and the MCU (Fig. 4). At first, the recruitment of different Ca^{2+} extrusion mechanisms was investigated using a relatively low pattern of activity consisting of 3 APs, which evoked well-defined bAP-CaTs in all interneurons tested (n = 65 cells; Fig. 4B–E). As PMCA can be partially inhibited by blocking its activator calmodulin with calmidazolium [12,14], we included this pharmacological agent in the intracellular recording solution (20 µM; Fig. 4A, B). Calmidazolium had no effect on the AP properties (Fig. 4A, B) or the bAP-CaT peak amplitude (ΔG/R peak amplitude in control: 0.14 ± 0.02, n = 13; ΔG/R peak amplitude in calmidazolium: 0.11 ± 0.01, n = 9; $P > 0.05$, Mann-Whitney test, Fig. 4B, G) but prolonged the bAP-CaT decay time constant (decay τ in control: 356 ± 71 ms, n = 11; decay τ in calmidazolium: 706 ± 163 ms, n = 9; $P < 0.05$, Mann-Whitney test, Fig. 4C, H), indicating that PMCA is involved in dendritic Ca^{2+} clearance at low levels of activity. To examine the role of the NCX, we replaced extracellular Na^+ with Li^+ ions that are not transported by the exchanger and, thus, make it nonoperational (Fig. 4D; [12,37]). The presence of Li^+ had no impact on the AP properties (Fig. 4A, B) or the bAP-CaTs amplitude (Fig. 4G) but substantially increased the decay time (decay τ in control: 505 ± 137 ms, n = 5; decay τ in Li^+: 845 ± 238 ms, n = 5; $P < 0.05$, Mann-Whitney test, Fig. 4D, H), indicating that NCX represents a second major Ca^{2+} extrusion mechanism in dendrites of interneurons. In addition, bAP-CaTs were significantly prolonged in the presence of the SERCA pump inhibitor CPA (30 µM; Fig. 4F, H), which also led to a significant decrease in the bAP-

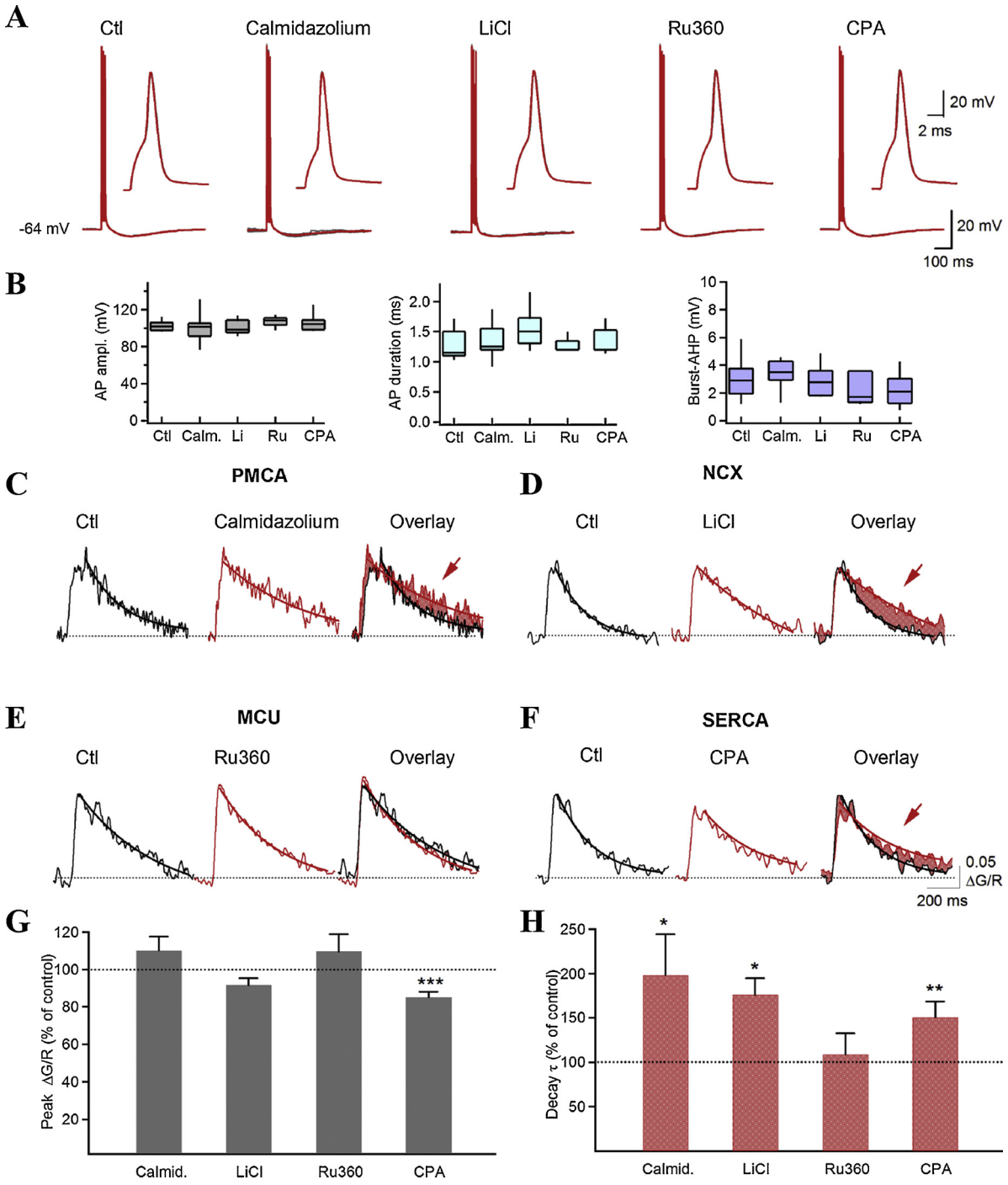

Fig. 4. Calcium extrusion mechanisms in dendrites of hippocampal CA1 interneurons.
(A–B) Sample traces of APs evoked by current injection in soma in control and in the presence of the PMCA inhibitor calmidazolium (20 μM), the NCX inhibitor lithium (100 mM), the MCU potent and selective inhibitor Ru360 (1 μM) or the SERCA pump antagonist CPA (30 μM), and summary box plots (B) showing the AP amplitude (left), the AP duration (middle) and the burst-AHP amplitude (right) under different pharmacological conditions. (C–F) Representative examples of bAP-CaTs evoked by 3 APs in control and in the presence of calmidazolium (C), lithium (D), Ru360 (E) or CPA (F). Red lines on CaT traces correspond to single exponential fits, red arrows pointing to the red shaded areas highlight the difference in the decay kinetics between control and pharmacological interventions (calmidazolium, LiCl or CPA). (G–H) Bar graphs of the bAP-CaT peak amplitude (G) and decay time constant (H) recorded in the presence of different pharmacological agents compared to control bAP-CaTs. *$P < 0.05$, **$P < 0.01$, ***$P < 0.001$, *t* test, Mann-Whitney test.

CaTs peak amplitude (ΔG/R peak amplitude in control: 0.12 ± 0.01, n = 18; ΔG/R peak amplitude in CPA: 0.09 ± 0.01, n = 18; $P < 0.001$, paired *t* test, Fig. 4F, H), indicating that SERCA-mediated Ca^{2+} release can contribute to bAP-CaTs. Similar to previous findings [38,39], the AP properties were not affected by the CPA application (Fig. 4A). Furthermore, blocking the MCU with a potent and selective channel inhibitor Ru360 [40,41] had no significant impact on the AP properties (AP amplitude, half-width and burst-afterhyperpolarization; Fig. 4A, B) or the bAP-CaTs peak amplitude and decay time constant (Fig. 4E, G, H), suggesting that MCU may not participate in Ca^{2+} clearance during low intracellular Ca^{2+} loads.

Given the activity-dependent enhancement of Ca^{2+} clearance, we

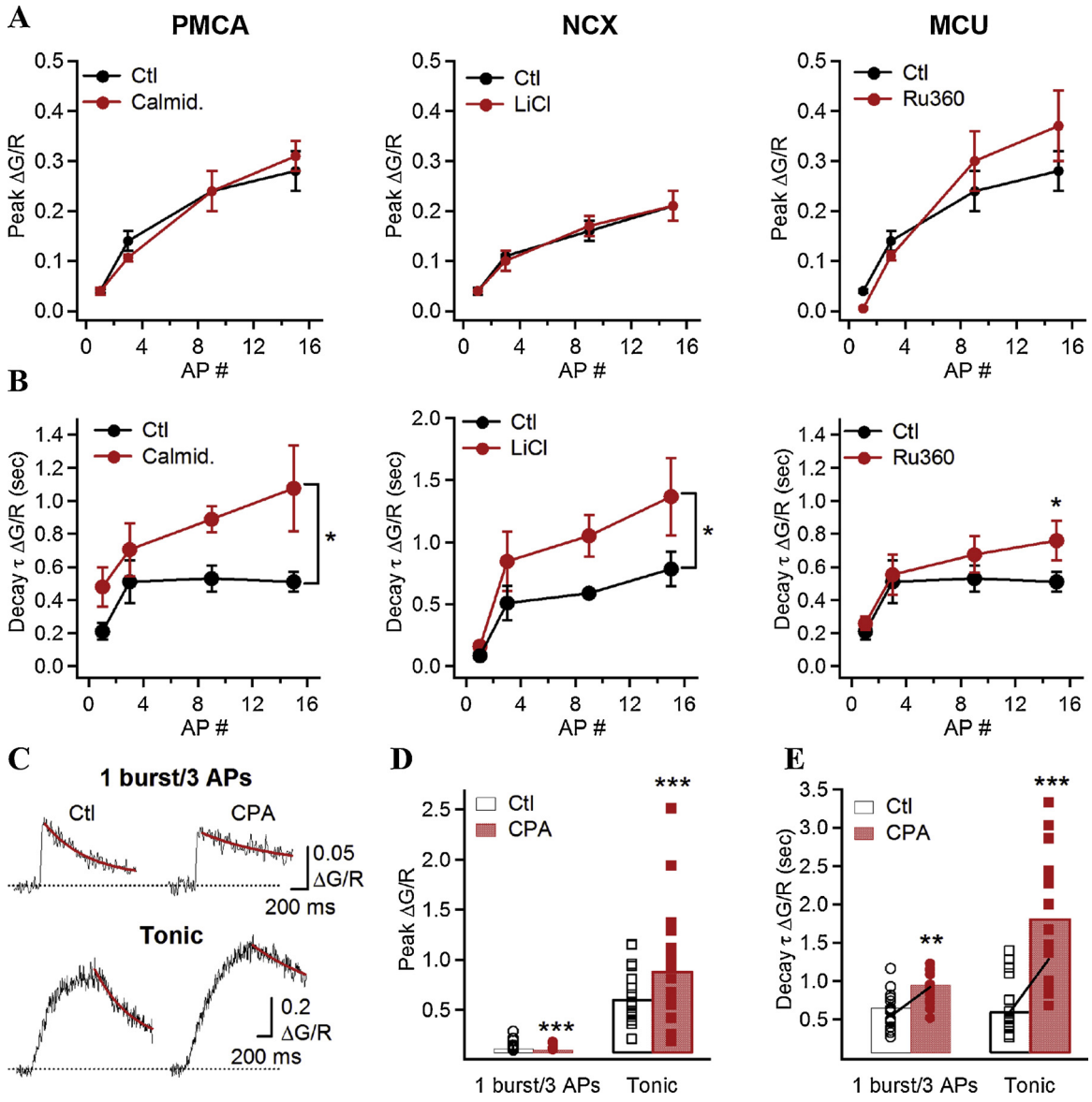

Fig. 5. Activity-dependent recruitment of the calcium extrusion mechanisms in interneurons.
(A–B) Summary plots showing the changes in the bAP-CaT peak amplitude (A) and decay time constant (B) as a function of number of APs in control (black) and during different pharmacological interventions (red). (C) Representative examples of bAP-CaTs evoked by 3 APs (top) and by tonic firing (1 s; bottom) in control (left) and in the presence of the SERCA pump inhibitor CPA (right). Red lines on CaT traces correspond to single exponential fits. (D–E) Bar graphs of the bAP-CaT peak amplitude (D) and decay time constant (E) recorded in control (black) and in the presence of CPA (red) during two activity patterns (1 burst of 3 APs and tonic firing). Lines connecting values on E correspond to CaT examples illustrated in C. $^{*}P < 0.05$, $^{**}P < 0.01$, $^{***}P < 0.001$, ANOVA.

investigated how these Ca^{2+} extrusion mechanisms may shape dendritic Ca^{2+} dynamics during repetitive neuronal activity. bAP-CaTs evoked by single APs and bursts of 3 APs applied at theta-frequency (1, 3 and 5 bursts) were compared in control and in the presence of pharmacological agents (Fig. 5). First, our data showed that blocking the PMCA, NCX or MCU had no impact on the bAP-CaTs peak amplitude at all firing patterns tested (Fig. 5A, $P > 0.05$, Mann-Whitney test). However, there were significant differences in the contribution of these mechanisms to the bAP-CaTs decay (Fig. 5B). In particular, inhibiting PMCA with calmidazolium delayed decay tau at all activity patterns (control: n = 13, calmidazolium: n = 9; $P < 0.05$, ANOVA; Fig. 5B, left), indicating that PMCA in interneurons provides for Ca^{2+} extrusion at a relatively wide range of cytosolic Ca^{2+} levels. In contrast, the NCX and MCU were only involved in Ca^{2+} extrusion at higher levels of activity, with the NCX being activated starting form 3 APs (Fig. 4H; 5B, center) and the MCU only starting from 5 bursts of 3 APs (15 APs in total; decay τ in control: 514 ± 58 ms, n = 13; decay τ in Ru360: 759 ± 125 ms, n = 4; $P < 0.05$, ANOVA; Fig. 5B, right). Furthermore, blocking the SERCA pump slowed down the Ca^{2+} extrusion not only at the low patterns of activity (1 burst of 3 APs; Figs. 4F, H, 5 C, E) but also during tonic firing of interneurons when CPA administration resulted in almost 3-fold prolongation of bAP-CaTs decay (decay τ in control: 614 ± 76 ms, n = 20; decay τ in CPA: 1 821 ± 196 ms, n = 18; $P < 0.001$, paired *t* test, Fig. 5C, E). The latter was associated with a significant increase in the bAP-CaTs peak amplitude (Fig. 5D), consistent with a major impact of SERCA inhibition on intracellular Ca^{2+} accumulation during high levels of activity. Collectively, these data point to the activity-dependent division of labor between different Ca^{2+} extrusion mechanisms in dendrites of hippocampal interneurons, with PMCA and SERCA pump operating at a wide range of cytosolic Ca^{2+} concentrations and NCX/MCU activated by large Ca^{2+} loads.

4. Discussion

In this study, we combined whole-cell patch-clamp recordings with dendritic Ca^{2+} imaging to examine the mechanisms of Ca^{2+} extrusion in dendrites of hippocampal CA1 RAD interneurons. While whole-cell patch-clamp recordings are associated with an extensive washout of the intracellular milieu in perisomatic compartments, it remains the only method allowing for simultaneous electrophysiological recordings from soma and Ca^{2+} imaging from dendrites. Through equilibrium between the cell cytoplasm and the pipette solution, it allows to obtain quantitative measurements of Ca^{2+} dynamics in small dendritic compartments [2]. Our data indicate that, dependent on the activity patterns, Ca^{2+} accumulations in interneuron dendrites remain temporally confined due to activity-dependent recruitment of specific Ca^{2+} removal mechanisms. The PMCA, NCX, SERCA and MCU were involved in Ca^{2+} extrusion, as inhibiting these mechanisms had a significant impact on the decay time constant of dendritic Ca^{2+} elevations and, in some cases (e.g., SERCA) on their amplitude. These results indicate that multiple Ca^{2+} extrusion mechanisms cooperate in interneurons dendrites and may control the induction and expression of Ca^{2+} -dependent forms of synaptic plasticity, cell energy and vulnerability to excitotoxicity through activity-dependent regulation of intracellular Ca^{2+} signaling.

bAP-CaTs in interneuron dendrites were shaped via activity-dependent recruitment of the Ca^{2+} extrusion mechanisms. At rest and during single APs, only PMCA was involved in Ca^{2+} clearance. However, as soon as the firing of interneurons was increased, additional extrusion mechanisms were activated, including the NCX and, at higher activity levels, the MCU. As a result, bAP-CaTs exhibited a similar decay across different patterns of interneuron firing, pointing to the efficient Ca^{2+} clearance during physiological activity. Under such conditions, the magnitude and duration of dendritic Ca^{2+} elevations were determined by the duration of stimulation and the properties of Ca^{2+} sources being activated.

Some Ca^{2+} extrusion mechanisms detected here in interneuron dendrites were similar to those operating in dendrites and spines of pyramidal cells. Indeed, PMCA and NCX were shown to cooperate in Ca^{2+} removal from the cytoplasm of hippocampal CA1 pyramidal neurons [12]. Furthermore, similar to findings in dendrites and spines of CA1 pyramidal cells [12], bAP-CaTs in interneurons showed activity-dependent slowing down, which required high intracellular Ca^{2+} concentration and was likely expressed via Ca^{2+} -dependent down-regulation of the PMCA activity. The PMCA exists in four isoforms, with PMCA1/4 expressed ubiquitously and PMCA2/3 expressed mainly in the central nervous system. The PMCA1 gene *Atp2b1* is mainly expressed in CA1 pyramidal cells whereas the PMCA2/3 genes *Atp2b2* and *Atp2b3* are also detected in CA1 interneurons (Allen Mouse Brain Atlas, 2004), indicating that PMCA2 and 3 could mediate Ca^{2+} extrusion in interneurons. In addition, more than 30 variants are generated through alternative splicing with yet unknown physiological functions, indicating that PMCAs can be a part of multi-signaling Ca^{2+} complexes [42,43]. The NCX1, NCX2 and NCX3 detected in the hippocampus [44,45] could all be expressed in interneurons and, due to their lower Ca^{2+} affinity, contribute to clearance of higher Ca^{2+} loads [17]. However, we found that both NCX and PMCA cooperate in Ca^{2+} extrusion at a relatively wide range of Ca^{2+} concentrations generated by different interneuron firing patterns. Moreover, we report a significant role of SERCA in interneuron dendritic Ca^{2+} extrusion. This is in contrast to pyramidal cells where Ca^{2+} uptake by SERCA pumps plays only a minor role [46]. Furthermore, the MCU was involved in Ca^{2+} removal during repetitive theta-burst activity. Interneurons contain the largest number of mitochondria in the brain [47,48], which may be critical for higher energy demands, ATP production and GABA metabolism in these cells [25,49,50]. Our findings support this view by providing evidence that mitochondria in interneurons may uptake high loads of cytosolic Ca^{2+} during repetitive high-frequency firing associated with hippocampal oscillations [50].

Under physiological conditions, repetitive firing of interneurons is required for induction of multiple forms of synaptic plasticity and regulation of neuronal excitability [31,51–54]. It is involved in generation of postsynaptic Ca^{2+} signals through activation of different mechanisms, including voltage-gated Ca^{2+} channels and intracellular Ca^{2+} stores. In addition, when coupled with synaptic activity, interneuron firing facilitates Ca^{2+} signals via glutamate receptors that rely on membrane depolarization [55,56]. Our findings suggest that Ca^{2+} extrusion mechanisms operating in interneuron dendrites, through local regulation of Ca^{2+} signal decay, may also play a role in controlling synaptic plasticity in interneurons. For example, some PMCA isoforms have been shown to bind with PSD-95 [57] and are, therefore, well positioned to control the Ca^{2+} dependent plasticity at excitatory synapses of interneurons. It is to be noted that inhibition of any of the Ca^{2+} extrusion mechanism tested here, or its possible depression under physiological conditions, can result in a significant prolongation of Ca^{2+} signals. Moreover, such prolongation in case of the SERCA pump inhibition was able to increase the temporal summation of Ca^{2+} elevations and the overall accumulation of postsynaptic Ca^{2+} ions. As high amplitude postsynaptic Ca^{2+} signals lead to increase in synaptic strength [58], SERCA pump inhibition may in some cases facilitate the induction of long-term potentiation in interneurons [32].

Furthermore, by maintaining intracellular Ca^{2+} homeostasis, Ca^{2+} extrusion mechanisms in interneurons may control apoptosis. For example, dysfunction or decreased expression of PMCA and NCX can lead to significant Ca^{2+} overloads and eventual cell death during aging, epileptogenesis and neurodegeneration [59,60]. Moreover, Ca^{2+} uptake to mitochondria controls the release of reactive oxygen species (ROS). As a result, under pathological conditions, excessive accumulation of cytosolic Ca^{2+} and/or alterations in the expression of Ca^{2+} binding/extrusion proteins in interneurons may lead to mitochondrial Ca^{2+} overload and significant production of ROS and nitric oxide [61]. Increased ROS generation together with alterations of anti-oxidative mechanisms may be in charge of oxidative stress, with far-reaching consequences for mitochondrial and nuclear DNA [61,62]. Thus, interneuron-specific Ca^{2+} extrusion mechanisms may play an additional role in interneuron-selective vulnerability during excitotoxicity as well as neurological and neurodegenerative conditions.

Author contributions statement

SC and AZM performed experiments, all authors analyzed the data and wrote the manuscript.

Conflict of interest statement

The authors declare that they have no conflict of interest.

Acknowledgements

We thank Dimitry Topolnik for excellent technical assistance. This work was supported by the Natural Sciences and Engineering Research Council of Canada (NSERC). SC was supported by a MSc Fellowship from the Fonds de Recherche Santé Québec (FRQS).

References

[1] B.L. Sabatini, M. Maravall, K. Svoboda, Ca2+ signaling in dendritic spines, Curr. Opin. Neurobiol. 11 (2001) 349–356.
[2] R. Yasuda, E.A. Nimchinsky, V. Scheuss, T.A. Pologruto, T.G. Oertner, B.L. Sabatini, K. Svoboda, Imaging calcium concentration dynamics in small neuronal compartments, Sci. STKE 2004 (2004) pl5.
[3] O. Camiré, L. Topolnik, Functional compartmentalisation and regulation of postsynaptic Ca2+ transients in inhibitory interneurons, Cell Calcium 52 (2012) 339–346.
[4] J.P. Gardner, M. Balasubramanyam, Na-Ca exchange in circulating blood cells, Ann. N. Y. Acad. Sci. 779 (1996) 502–514.
[5] O.H. Petersen, Localization and regulation of Ca2+ entry and exit pathways in

exocrine gland cells, Cell Calcium 33 (2003) 337–344.
[6] W.F. Graier, M. Frieden, R. Malli, Mitochondria and Ca(2+) signaling: old guests, new functions, Pflugers Arch. 455 (2007) 375–396.
[7] C. Pott, S.A. Henderson, J.I. Goldhaber, K.D. Philipson, Na+/Ca2+ exchanger knockout mice: plasticity of cardiac excitation-contraction coupling, Ann. N. Y. Acad. Sci. 1099 (2007) 270–275.
[8] A. Verkhratsky, V. Parpura, Calcium signalling and calcium channels: evolution and general principles, Eur. J. Pharmacol. 739 (2014) 1–3.
[9] H.F. Deluca, G.W. Engstrom, Calcium uptake by rat kidney mitochondria, Proc. Natl. Acad. Sci. U. S. A. 47 (1961) 1744–1750.
[10] F. Fieni, S.B. Lee, Y.N. Jan, Y. Kirichok, Activity of the mitochondrial calcium uniporter varies greatly between tissues, Nat. Commun. 3 (2012) 1317.
[11] M.P. Blaustein, W.J. Lederer, Sodium/calcium exchange: its physiological implications, Physiol. Rev. 79 (1999) 763–854.
[12] V. Scheuss, R. Yasuda, A. Sobczyk, K. Svoboda, Nonlinear [Ca2+] signaling in dendrites and spines caused by activity-dependent depression of Ca2+ extrusion, J. Neurosci. 26 (2006) 8183–8194.
[13] D.H. MacLennan, W.J. Rice, N.M. Green, The mechanism of Ca2+ transport by sarco(endo)plasmic reticulum Ca2+-ATPases, J. Biol. Chem. 272 (1997) 28815–28818.
[14] H. Markram, P.J. Helm, B. Sakmann, Dendritic calcium transients evoked by single back-propagating action potentials in rat neocortical pyramidal neurons, J. Physiol. (Paris) 485 (1995) 1–20.
[15] J.L. Werth, Y.M. Usachev, S.A. Thayer, Modulation of calcium efflux from cultured rat dorsal root ganglion neurons, J. Neurosci. 16 (1996) 1008–1015.
[16] M. Brini, E. Carafoli, The plasma membrane Ca^2+ ATPase and the plasma membrane sodium calcium exchanger cooperate in the regulation of cell calcium, Cold Spring Harb. Perspect. Biol. (3/pii) (2011) a004168.
[17] M.P. Blaustein, M. Juhaszova, V.A. Golovina, P.J. Church, E.F. Stanley, Na/Ca exchanger and PMCA localization in neurons and astrocytes: functional implications, Ann. N. Y. Acad. Sci. 976 (2002) 356–366.
[18] Y. Kirichok, G. Krapivinsky, D.E. Clapham, The mitochondrial calcium uniporter is a highly selective ion channel, Nature 427 (2004) 360–364.
[19] I. Drago, D. De Stefani, R. Rizzuto, T. Pozzan, Mitochondrial Ca2+ uptake contributes to buffering cytoplasmic Ca2+ peaks in cardiomyocytes, Proc. Natl. Acad. Sci. U. S. A. 109 (2012) 12986–12991.
[20] R. Rizzuto, P. Pinton, W. Carrington, F.S. Fay, K.E. Fogarty, L.M. Lifshitz, R.A. Tuft, T. Pozzan, Close contacts with the endoplasmic reticulum as determinants of mitochondrial Ca2+ responses, Science 280 (1998) 1763–1766.
[21] R.M. Empson, M.L. Garside, T. Knöpfel, Plasma membrane Ca2+ ATPase 2 contributes to short-term synapse plasticity at the parallel fiber to Purkinje neuron synapse, J. Neurosci. 27 (2007) 3753–3758.
[22] D. Jeon, Y.M. Yang, M.J. Jeong, K.D. Philipson, H. Rhim, H.S. Shin, Enhanced learning and memory in mice lacking Na+/Ca 2+ exchanger 2, Neuron 38 (2003) 965–976.
[23] J. Qiu, Y.W. Tan, A.M. Hagenston, M.A. Martel, N. Kneisel, P.A. Skehel, D.J. Wyllie, H. Bading, G.E. Hardingham, Mitochondrial calcium uniporter Mcu controls excitotoxicity and is transcriptionally repressed by neuroprotective nuclear calcium signals, Nat. Commun. 4 (2013) 2034.
[24] R. Rizzuto, D. De Stefani, A. Raffaello, C. Mammucari, Mitochondria as sensors and regulators of calcium signalling, Nat. Rev. Mol. Cell Biol. 13 (2012) 566–578.
[25] G.S. Williams, L. Boyman, W.J. Lederer, Mitochondrial calcium and the regulation of metabolism in the heart, J. Mol. Cell. Cardiol. 78 (2015) 35–45.
[26] J.R. Marland, P. Hasel, K. Bonnycastle, M.A. Cousin, Mitochondrial calcium uptake modulates synaptic vesicle endocytosis in central nerve terminals, J. Biol. Chem. 291 (2016) 2080–2086.
[27] H. Schmidt, O. Arendt, J. Eilers, Diffusion and extrusion shape standing calcium gradients during ongoing parallel fiber activity in dendrites of Purkinje neurons, Cerebellum 11 (2012) 694–705.
[28] T.F. Freund, G. Buzsáki, Interneurons of the hippocampus, Hippocampus 6 (1996) 347–470.
[29] S.-H. Lee, C. Rosenmund, B. Schwaller, E. Neher, Differences in Ca2+ buffering properties between excitatory and inhibitory hippocampal neurons from the rat, J. Physiol. 525 (2000) 405–418.
[30] J.H. Goldberg, G. Tamas, D. Aronov, R. Yuste, Calcium microdomains in aspiny dendrites, Neuron 40 (2003) 807–821.
[31] L. Topolnik, Dendritic calcium mechanisms and long-term potentiation in cortical inhibitory interneurons, Eur. J. Neurosci. 35 (2012) 496–506.
[32] O. Camiré, L. Topolnik, Dendritic calcium nonlinearities switch the direction of synaptic plasticity in fast-spiking interneurons, J. Neurosci. 34 (2014) 3864–3877.
[33] O. Camiré, L. Topolnik, Two-photon calcium imaging in neuronal dendrites in brain slices, JoVe 133 (2018), https://doi.org/10.3791/56776.
[34] A. Evstratova, S. Chamberland, L. Topolnik, Cell type-specific and activity-dependent dynamics of action potential-evoked Ca2+ signals in dendrites of hippocampal inhibitory interneurons, J. Physiol. 589 (2011) 1957–1977.
[35] M. Kisfali, T. Lrincz, E.S. Vizi, Comparison of Ca2+ transients and [Ca2+]i in the dendrites and boutons of non-fast-spiking GABAergic hippocampal interneurons using two-photon laser microscopy and high- and low-affinity dyes, J. Physiol. 591 (2013) 5541–5553.
[36] T. Klausberger, L.F. Marton, J. O'Neill, J.H. Huck, Y. Dalezios, P. Fuentealba, W.Y. Suen, E. Papp, T. Kaneko, M. Watanabe, J. Csicsvari, P. Somogyi, Complementary roles of cholecystokinin- and parvalbumin-expressing GABAergic neurons in hippocampal network oscillations, J. Neurosci. 25 (2005) 9782–9793.
[37] R.M. Mulkey, R.S. Zucker, Posttetanic potentiation at the crayfish neuromuscular junction is dependent on both intracellular calcium and sodium ion accumulation, J. Neurosci. 12 (1992) 4327–4336.
[38] E.J. Nelson, R. Bangalore, T. Benson, R.S. Kass, P.M. Hinkle, Inhibition of L-type calcium channel activity by thapsigargin and 2,5-t-butylhydroquinone, but not by cyclopiazonic acid, Biochem. J. 302 (1994) 147–154.
[39] V.M. Sandler, J.G. Barbara, Calcium-induced calcium release contributes to action potential-evoked calcium transients in hippocampal CA1 pyramidal neurons, J. Neurosci. 19 (1999) 4325–4336.
[40] M.A. Matlib, Z. Zhou, S. Knight, S. Ahmed, K.M. Choi, J. Krause-Bauer, R. Phillips, R. Altschuld, Y. Katsube, N. Sperelakis, D.M. Bers, Oxygen-bridged dinuclear ruthenium amine complex specifically inhibits Ca2+ uptake into mitochondria in vitro and in situ in single cardiac myocytes, J. Biol. Chem. 273 (1998) 10223–10231.
[41] J.Q. Kwong, X. Lu, R.N. Correll, J.A. Schwanekamp, R.J. Vagnozzi, M.A. Sargent, A.J. York, J. Zhang, D.M. Bers, J.D. Molkentin, The mitochondrial calcium uniporter selectively matches metabolic output to acute contractile stress in the heart, Cell Rep. 12 (2015) 15–22.
[42] T. Domi, F. Di Leva, L. Fedrizzi, A. Rimessi, M. Brini, Functional specificity of PMCA isoforms? Ann. N. Y. Acad. Sci. 1099 (2007) 237–246.
[43] E.E. Strehler, Plasma membrane calcium ATPases: from generic Ca(2+) sump pumps to versatile systems for fine-tuning cellular Ca(2+), Biochem. Biophys. Res. Commun. 460 (2015) 26–33.
[44] A. Canitano, M. Papa, F. Boscia, P. Castaldo, S. Sellitti, M. Taglialatela, L. Annunziato, Brain distribution of the Na+/Ca2+ exchanger-encoding genes NCX1, NCX2, and NCX3 and their related proteins in the central nervous system, Ann. N. Y. Acad. Sci. 976 (2002) 394–404.
[45] M. Papa, A. Canitano, F. Boscia, P. Castaldo, S. Sellitti, H. Porzig, M. Taglialatela, L. Annunziato, Differential expression of the Na+-Ca 2+ exchanger transcripts and proteins in rat brain regions, J. Comp. Neurol. 461 (31) (2003) 48.
[46] Z.F. Mainen, R. Malinow, K. Svoboda, Synaptic calcium transients in single spines indicate that NMDA receptors are not saturated, Nature. 399 (1999) 151–155.
[47] G.H. Kageyama, M.T. Wong-Riley, Histochemical localization of cytochrome oxidase in the hippocampus: correlation with specific neuronal types and afferent pathways, Neuroscience 7 (1982) 2337–2361.
[48] A.I. Gulyás, G. Buzsáki, T.F. Freund, H. Hirase, Populations of hippocampal inhibitory neurons express different levels of cytochrome c, Eur. J. Neurosci. 23 (2006) 2581–2594.
[49] C. Huchzermeyer, N. Berndt, H.G. Holzhütter, O. Kann, Oxygen consumption rates during three different neuronal activity states in the hippocampal CA3 network, J. Cereb. Blood Flow Metab. 33 (2013) 263–271.
[50] O. Kann, I.E. Papageorgiou, A. Draguhn, Highly energized inhibitory interneurons are a central element for information processing in cortical networks, J. Cereb. Blood Flow Metab. 34 (2014) 1270–1282.
[51] K.P. Lamsa, D.M. Kullmann, M.A. Woodin, Spike-timing dependent plasticity in inhibitory circuits, Front. Synaptic Neurosci. 2 (2010) 8, https://doi.org/10.3389/fnsyn.2010.00008.
[52] F. Laezza, R. Dingledine, Induction and expression rules of synaptic plasticity in hippocampal interneurons, Neuropharmacology 60 (2011) 720–729.
[53] O. Camiré, J.C. Lacaille, L. Topolnik, Dendritic signaling in inhibitory interneurons: local tuning via group I metabotropic glutamate receptors, Front. Physiol. 3 (2012) 259, https://doi.org/10.3389/fphys.2012.00259.
[54] P.Y. Lau, L. Katona, P. Saghy, K. Newton, P. Somogyi, K.P. Lamsa, Long-term plasticity in identified hippocampal GABAergic interneurons in the CA1 area in vivo, Brain Struct. Funct. 222 (2017) 1809–1827.
[55] K. Lamsa, J.H. Heeroma, D.M. Kullmann, Hebbian LTP in feed-forward inhibitory interneurons and the temporal fidelity of input discrimination, Nat. Neurosci. 8 (2005) 916–924.
[56] L. Topolnik, M. Azzi, F. Morin, A. Kougioumoutzakis, J.C. Lacaille, mGluR1/5 subtype-specific calcium signalling and induction of long-term potentiation in rat hippocampal oriens/alveus interneurones, J. Physiol. 575 (2006) 115–131.
[57] S.J. DeMarco, E.E. Strehler, Plasma membrane Ca2_-atpase isoforms 2b and 4b interact promiscuously and selectively with members of the membrane-associated guanylate kinase family of PDZ (PSD95/Dlg/ ZO-1) domain-containing proteins, J. Biol. Chem. 276 (2001) 21594–21600.
[58] S.N. Yang, Y.G. Tang, R.S. Zucker, Selective induction of LTP and LTD by postsynaptic [Ca 2+]i elevation, J. Neurophysiol. 81 (1999) 781–787.
[59] S.O. Ketelaars, J.A. Gorter, E. Aronica, W.J. Wadman, Calcium extrusion protein expression in the hippocampal formation of chronic epileptic rats after kainate-induced status epilepticus, Epilepsia 45 (2004) 1189–1201.
[60] E.E. Strehler, S.A. Thayer, Evidence for a role of plasma membrane calcium pumps in neurodegenerative disease: recent developments, Neurosci. Lett. 663 (2018) 39–47.
[61] O. Kann, R. Kovács, Mitochondria and neuronal activity, Am. J. Physiol. Cell Physiol. 292 (2007) C641–57.
[62] P. Steullet, J.H. Cabungcal, A. Kulak, R. Kraftsik, Y. Chen, T.P. Dalton, M. Cuenod, K.Q. Do, Redox dysregulation affects the ventral but not dorsal hippocampus: impairment of parvalbumin neurons, gamma oscillations, and related behaviors, J. Neurosci. 30 (2010) 2547–2558.